IEICE TRANS. COMMUN., VOL.E107–B, NO.1 JANUARY 2024

PAPER

Investigation of a Non-Contact Bedsore Detection System*

Tomoki CHIBA[†a)], ***Student Member***, **Yusuke ASANO**[†], ***Nonmember***, ***and*** **Masaharu TAKAHASHI**[††], ***Fellow***

SUMMARY The proportion of persons over 65 years old is projected to increase worldwide between 2022 and 2050. The increasing burden on medical staff and the shortage of human resources are growing problems. Bedsores are injuries caused by prolonged pressure on the skin and stagnation of blood flow. The more the damage caused by bedsores progresses, the longer the treatment period becomes. Moreover, patients require surgery in some serious cases. Therefore, early detection is essential. In our research, we are developing a non-contact bedsore detection system using electromagnetic waves at 10.5 GHz. In this paper, we extracted appropriate information from a scalogram and utilized it to detect the sizes of bedsores. In addition, experiments using a phantom were conducted to confirm the basic operation of the bedsore detection system. As a result, using the approximate curves and lines obtained from prior analysis data, it was possible to estimate the volume of each defected area, as well as combinations of the depth of the defected area and the length of the defected area. Moreover, the experiments showed that it was possible to detect bedsore presence and estimate their sizes, although the detection results had slight variations.

key words: *bedsore detection, Finite Integration Technique (FIT), non-contact detection, wavelet transforms*

1. Introduction

The population in Japan aged over 65 years old reached 36.21 million out of a total population of 125.5 million as of October 2021. This is equivalent to a ratio of elderly to total population of 28.9%, which is the highest ratio in the world [1]. The proportion of persons over 65 years old is projected to increase worldwide between 2022 and 2050. Even at the global level in 2022, approximately 10% of people are aged over 65 years old [2]. Therefore, the demand for medical care and long-term care will rise. The increase in social security costs is having a serious impact on the nation's finances; moreover, the increasing burden on medical staff and the shortage of human resources are growing problems [3].

Bedsores, also called pressure ulcers, are localized skin and subcutaneous tissue injuries caused by prolonged pressure and stagnation of blood flow. This is mainly seen in bedridden elderly people. Once bedsores develop, the skin damage progresses gradually unless appropriate measures are taken. Although surgery is required to treat bedsores in late-stages, early detection and treatment can shorten the duration of treatment. To prevent occurrence of bedsores or its worsening, it is necessary to change the patient's position at regular intervals and introduce pressure-dispersing devices such as air mattresses and cushions [4]. As home medical care increases in the near future, a system to detect bedsores for caregivers without expertise and in telemedicine will become necessary.

There are some existing evaluation methods for bedsores, including NPUAP (National Pressure Ulcer Advisory Panel), which mainly classifies bedsores into four stages based on the progression of damage as follows. Stage I: Non blanchable Erythema; Stage II: Partial Thickness Skin Loss; Stage III: Full Thickness Skin Loss; and Stage IV: Full Thickness Tissue Loss [4].

In the past, contact sensors [5]–[8], non-contact sensors [9], and pressure measurement using fabric sensors with conductive fibers [10] have been investigated for the detection of skin diseases such as bedsores and lesions caused by diseases deep in the skin.

In our prior paper, we used a patch antenna operating at 10.5 GHz and found that the difference in reflection coefficient enables the identification of bedsores at Stages II–IV [11]. However, this method works only under specific situations where the distance between a model and an antenna is fixed. In our other previous papers, wavelet transforms of voltage waveforms were shown to be effective for stage identification [12], [13].

2. Simulation

2.1 Assumed System and Antenna

The assumed system is shown in Fig. 1. This system is comprised of two parts: a patch antenna that transmits and receives microwaves, and a control unit that supplies power and processes information. The patch antenna is inserted under a mattress as shown in Fig. 1. This system is designed to detect bedsores in the sacral region, which is the most

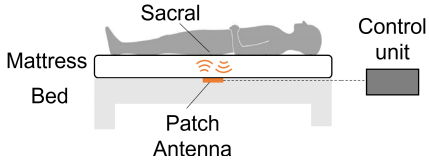

Fig. 1 Schematic diagram of the assumed system.

Manuscript received April 27, 2023.
Manuscript revised August 2, 2023.
Manuscript publicized September 12, 2023.

[†]The authors are with Graduate School of Science and Engineering, Chiba University, Chiba-shi, 263-8522 Japan.
[††]The author is with Center for Frontier Medical Engineering, Chiba-shi, 263-8522 Japan.

*This work was supported by JSPS KAKENHI Grant Number 2K12919.

a) E-mail: 23wm4202@student.gs.chiba-u.jp

DOI: 10.1587/transcom.2023EBP3070

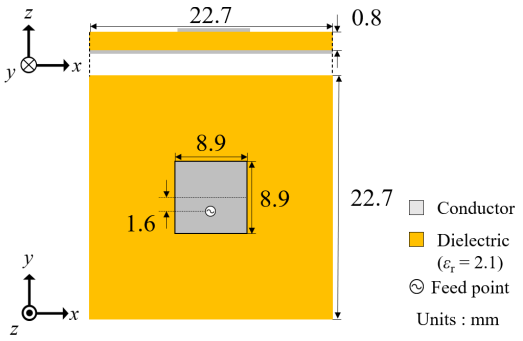

Fig. 2 Dimensions of the antenna.

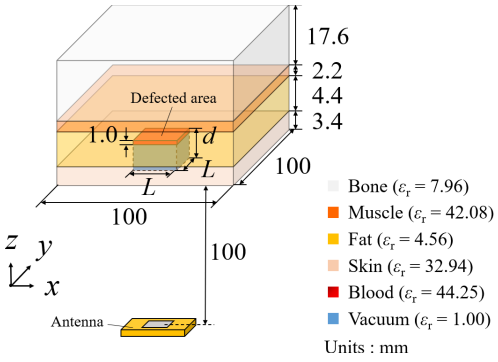

Fig. 3 General simulation model.

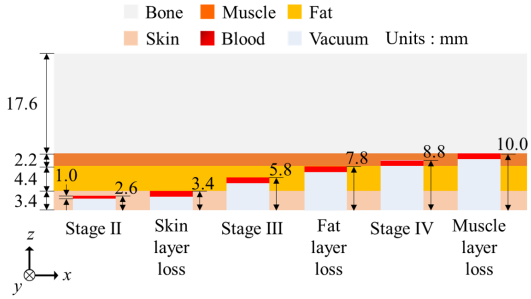

Fig. 4 Example image of the depth of the bedsores.

frequent site of bedsores. Therefore, the antenna element is set near the nadir of the sacral region.

The dimensions of the antenna are shown in Fig. 2. The patch antenna used in this paper can both transmit and receive. The operating frequency is 10.525 GHz, which was also used in our prior paper [12]. The frequency band of 10.5 to 10.55 GHz can be used for the Unlicensed Low-Power Service, and so we can use this band without license [14]. At this frequency band, the radio wave can enter the subcutaneous tissue and be monitored. In the present study, the center of this frequency band was used. The dielectric substrate is a PTFE that operates well in the high-frequency band. The power supply method is a rear mount coaxial power supply because of its simplicity in design and fabrication.

2.2 Simplified Skin Models

The general simulation model is shown in Fig. 3. This model is a simple rectangular model that is constructed of layers of skin, fat, muscle, and bone. The model simply simulates the skin tissue of the sacral region. As the stage of bedsore progresses, the defect becomes deeper. Therefore, we create a central defected area in the bedsore skin model and insert a blood layer at the bottom of the defect to simply reproduce a bedsore. The healthy skin model does not have a defected area. The thickness of each tissue and the depth of the defected area d are defined based on ultrasound images [15]. An example image of d is shown in Fig. 4. Based on the NPUAP/EPUAP stage classification of bedsores, we analyze a total of six bedsore models with different types of d: Stage II-IV, skin layer loss, fat layer loss, and muscle layer loss. For each model, we vary the length of the defected area L from 20 mm to 50 mm in 5 mm increments for analysis. Since this paper is only a basic study of the method, the input waveform to the antenna is a Gaussian pulse, and Finite Integration Technique (FIT) is used as the analysis method. The distance between the antenna and the model is set to 100 mm, considering the thickness of commercially available bedsore prevention mattresses. In addition, typical cloths fabrics are electrically almost the same as air. Therefore, nothing is inserted between the skin model and the antenna.

2.3 Detection Flow

This method required two types of approximations for bedsore detection to be obtained in advance. The detailed flow for approximations acquisition (Fig. 5) is described below. The basic method for obtaining a scalogram was the same as that proposed in our previous study [12].

Firstly, we obtained the voltage waveforms of the received waves from the healthy skin model and all bedsore skin models. This was equivalent to the (S_{11}) Real in the time domain that can be observed with the vector network analyzer used in the experiments, and was adopted because it facilitated comparison between the analysis and experiments. We then calculated the numerical difference between both waveforms and extracted only the waveform of bedsores. Figure 6 shows the voltage waveforms obtained from the healthy skin model and from the bedsore model, as well as a graph of the waveforms with the difference between the two waveforms.

Second, we applied wavelet transformation to the bedsore waveforms and obtained the scalograms. An example of an obtained scalogram is shown in Fig. 7. The wavelet transformation can obtain scalograms with different characteristics by selecting pieces of waves, called mother wavelets, for fitting. In this paper, Morse wavelet was used as the mother wavelet. The Morse wavelet was the mother wavelet implemented in MATLAB and was selected due to its high frequency resolution and time resolution.

Since it is difficult to directly compare the obtained

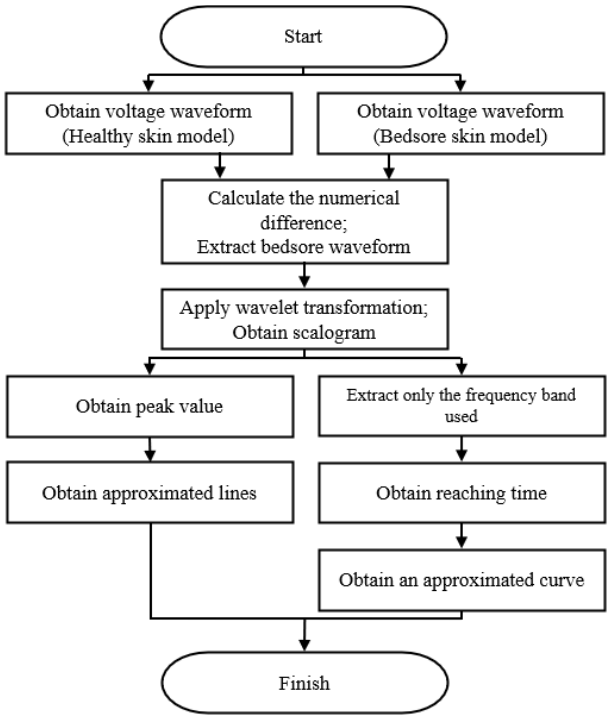

Fig. 5 Flow for approximations acquisition.

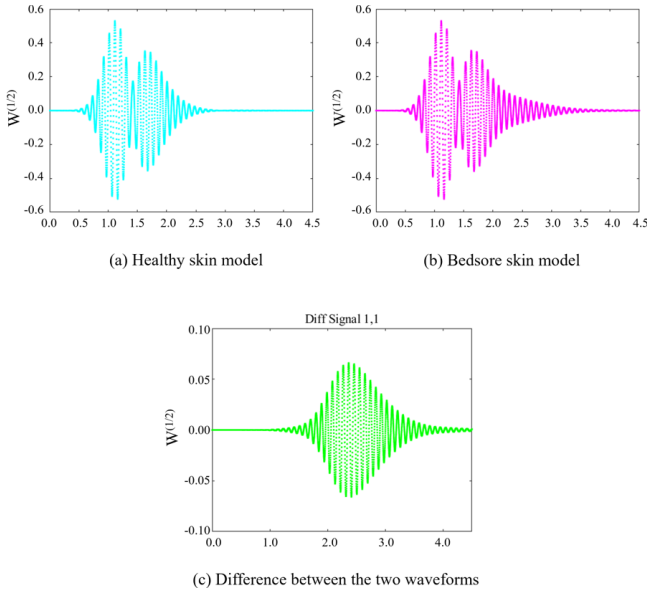

(a) Healthy skin model (b) Bedsore skin model

(c) Difference between the two waveforms

Fig. 6 Examples of voltage waveforms used.

scalograms, automatic bedsore detection requires some method to convert and extract the characteristics of the scalograms. Therefore, this method used two types of data: Peak value and Reaching time.

From the scalogram, only the frequency band used was extracted, and we obtained the time at which the value reached the set threshold (i.e., reaching time). Figure 8 shows an example. The dotted line indicates the threshold value, and the red asterisk indicates the reaching time. The

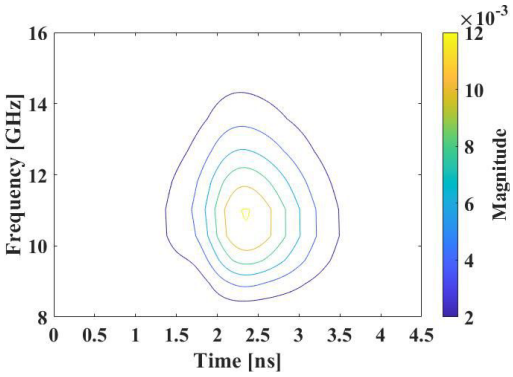

Fig. 7 Example of Scalogram.

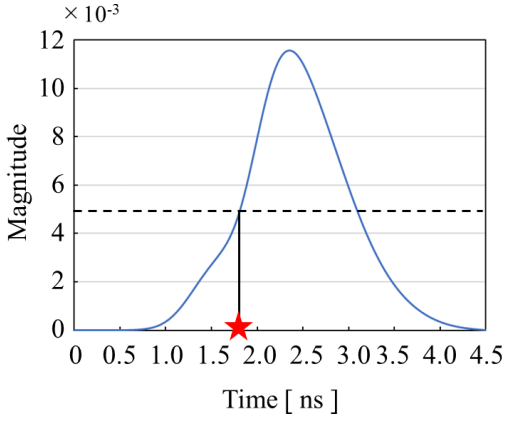

Fig. 8 Example of Reaching time.

threshold used in this paper is 5.0×10^3. This threshold was set to the smallest value in Fig. 8 for which the time to reach it was separated for all models. A total of 42 wavelet waveforms were analyzed for the six stages (depth of bedsores; d) shown in Fig. 4 and seven sizes of bedsores; L. The volume of each defected area was then calculated using d and L, and plotted as shown in Fig. 9. The peak value appearance time was not used because it lacked robustness due to the fact that a slight change in peak value caused a large change in appearance time. An approximate curve was generated (Fig. 9). As an elementary study, we used a fifth-order polynomial approximation to obtain the approximate curve. This curve made it possible to estimate the volume of the defected area using the reaching time.

From the scalogram, we obtained peak values and plotted by stage (Fig. 10). The peak value represents the maximum value of magnitude on the obtained scalogram. Figure 10 shows the approximate lines at each stage, but only the three stages defined in the NPUAP are shown for visibility. In this paper, the skin models were made in six stages in total, so six approximated lines were obtained. Therefore, it was possible to estimate L at each stage from the peak value by using the approximated line at each stage.

After acquiring two types of approximations, detection was performed according to the detection flow shown in Fig. 11. When actually detecting bedsores, the approximate

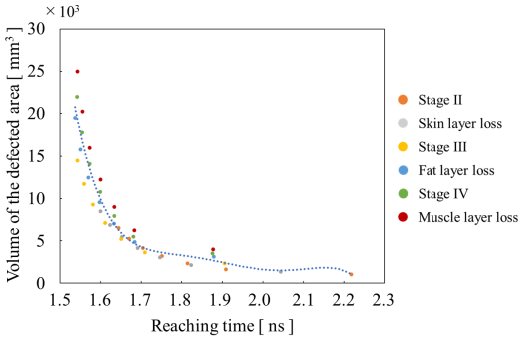

Fig. 9 Relationship between reaching time and volume of defected area and the approximate curve (dotted line).

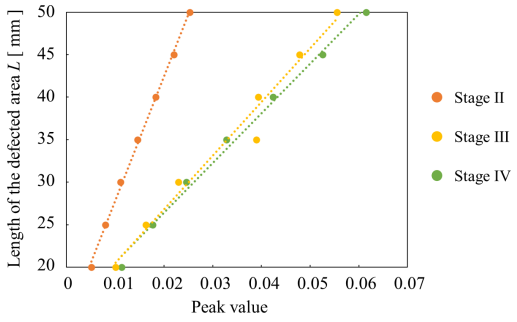

Fig. 10 Relationship between peak value and length of the defected area, and the approximated lines (only Stages II–IV shown as examples).

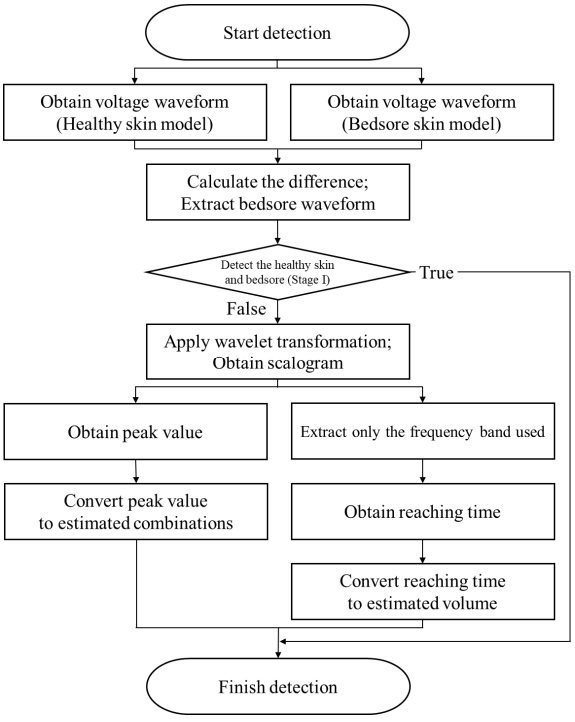

Fig. 11 Detection flow.

curves shown in Fig. 9 and Fig. 10 should be prepared in advance. The details are described below.

First, we obtained the voltage waveforms of the received waves from the healthy skin model and all bedsore skin models. We then calculated the difference between both waveforms (healthy and each bedsore model) to obtain only the waveforms of bedsores. When actually applied in a patient, the waveform in the healthy state (at the time of antenna installation or when the nurse determines) is stored as the healthy skin waveform, and the waveform acquired in real time is differentiated as the bedsore skin waveform for detection. For healthy skin waveforms, it is expected that the same area of the same patient will be stored at the time of equipment installation or at the time of confirmation by the nurse. If the difference in waveforms is larger than a given value, then a bedsore is detected. This difference appears even in stage I, when blood volume and other factors in the body change without changes on the skin surface.

Second, we applied wavelet transformation to the bedsore waveform, and obtained a scalogram. As shown in the flow chart in Fig. 5, we obtained the peak value and reaching time.

We converted the reaching time to the estimated volume of the defected area using the approximate curve shown in Fig. 9. Then, from the approximate straight lines and peak values shown in Fig. 10, we estimated the size L for each of the six stages shown in Fig. 4 and calculated the volume of the stages by depth d corresponding to each stage. This combination is henceforth referred to as the estimated combination.

Finally, from the candidate volumes for each stage obtained from Fig. 10, the one closest to the volume estimated in Fig. 9 was selected, and the depth d and estimated size L of the selected stage were determined as the final estimation result.

2.4 Simulation Results

An example of detection results is shown below. The bedsore model with $d = 3.0$, $L = 35$ was used for detection. The scalogram obtained from the wavelet transforms yielded a reaching time of 1.71 ns and peak value of 0.0178. Based on the reaching time, an estimated volume of 4048 mm^3 was obtained from the approximate curve in Fig. 9. Moreover, based on the peak value, estimated combinations of d and L were obtained from the approximate lines in Fig. 10. For example, assuming Stage III ($d = 5.8$), $L = 25$ was estimated from the peak value using the approximate line for Stage III. From the estimated combination, the volume of the defected area was calculated using d and L. For all stages, combinations were estimated using the same approach, and volumes of defected areas were calculated (Table 1). From the estimated combinations, we selected the combination with the closest volume to the estimated volume, which in this example is a detection result of $d = 2.6$ (Stage II) and $L = 39$.

Other detection results are shown in Table 2. Compared to the actual values, both d and L of all results had some errors. However, the presence of bedsores could be detected in all cases. For example, in the bedsore assessment tools in

Table 1 Example of estimated combinations.

d [mm]	L [mm]	volume [mm^3]
2.6	39	3955
3.4	33	3703
5.8	25	3625
7.8	25	4875
8.8	25	5500
10	25	6250

Table 2 Other detection results.

Actual values [mm]		Estimated combinations [mm]		Errors [mm]	
d	L	d	L	d	L
2.8	43	3.4 (S)	38	0.6	-5.0
3.2	25	5.8 (III)	21	2.6	-4.0
8.2	52	7.8 (F)	53	-0.4	1.0
4.7	27	7.8 (F)	24	3.1	-3.0
7.6	43	8.8 (IV)	43	1.2	0.0

S : Skin layer loss F : Fat layer loss
III : Stage III IV : Stage IV

Japan "DESIGN-R®2022" [16], the 'Depth' of the bedsore was not determined by a specific number, but by the tissue eroded. From this perspective, almost all results were able to estimate erosion to the same tissue. As for the 'Size', all results detected the correct L, since the steps progress every 20 mm. Therefore, it was possible to detect bedsores to the extent that they did not interfere at all with the actual assessment of bedsores.

3. Experiments

3.1 Fabricated Antenna

Experiments were conducted to verify the bedsore detection system proposed in the previous section. As mentioned earlier, a PTFE was used as the dielectric substrate for the design of the patch antenna. Therefore, in this paper, we used a PTFE substrate DiClad880 (manufactured by Rogers), which had a dielectric constant (ε_r) of 2.17 ± 0.02 and a thickness of 0.8 mm (copper foil thickness on both sides 18 µm). The fabricated antenna and its reflection coefficient (S_{11}) are shown in Fig. 12. The actual dimensions were slightly changed due to adjustments caused by manufacturing errors and environmental changes. S_{11} was -17.72 dB at 10.525 GHz, indicating good operation at the operating frequency. The fabricated antenna showed a similar tendency as those in the analysis; therefore, this antenna was adopted.

In this system, a wider bandwidth was needed to improve the distance resolution. However, the Japanese Radio Law currently imposes restrictions. Therefore, from Fig. 12, the system used a bandwidth of around ±0.3 GHz from 10.525 GHz.

3.2 Hybrid Phantom

In this paper, we used hybrid phantoms consisting of three layers: porcine skin, porcine back fat, and the TX-151 phantom. This was because it was considered difficult to reproduce the electrical constants of the skin and fat layers in the phantom. Figure 13 shows a graph of the electric field distribution with and without bone. Bone has little effect on detection because electromagnetic waves are mostly absorbed by bone up to the muscle layer. Therefore, the bone was completely replaced by the muscle layer. The following is a description of the preparation procedure for each layer.

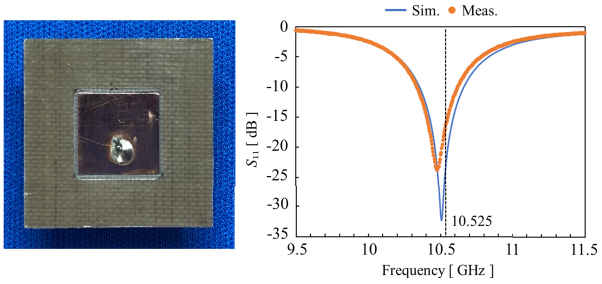

Fig. 12 Fabricated antenna.

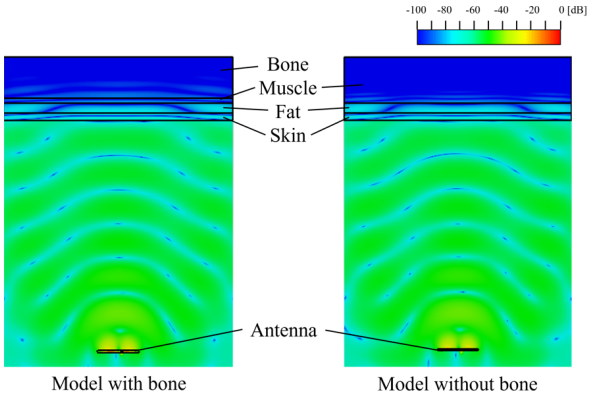

Fig. 13 Comparison of electric field distribution between models with and without bone.

First, the skin layer is explained. The surface of the porcine skin is covered with hair, so the skin was first lightly bathed in hot water, then pliers were used to remove the hair and prepare the skin surface. Thereafter, the skin pieces were cut to the desired size using stencils. Since the desired thickness had already been achieved, no special processing was performed on the thickness. One square skin was prepared as the healthy part and two square skins (L = 20, 30 mm) with the center cut out were prepared as the bedsore skin.

Second, the fat layer is explained. The backfat obtained was not in a form from which the desired shape could be extracted. Therefore, a mold of the desired shape was made and filled with finely cut fat fragments. As with the skin layer, one square fat was prepared as the healthy skin and two square fats (L = 20, 30 mm) with the center cut out were prepared as the bedsore skin.

Third, the muscle layer and blood layer are explained. As mentioned earlier, the presence or absence of bone had little effect on detection. Therefore, for simplicity, we replaced all the originally bony parts with muscles. Since

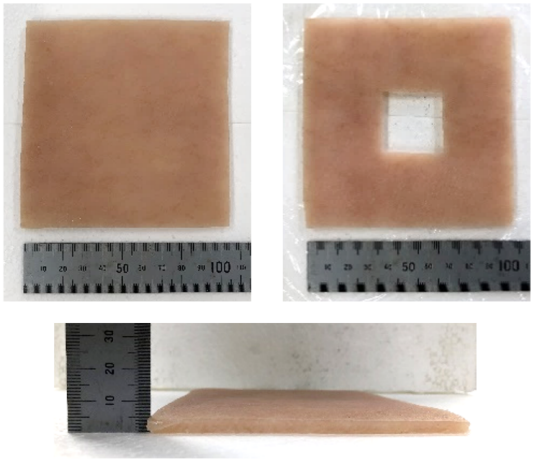

Fig. 14 Processed porcine skin.

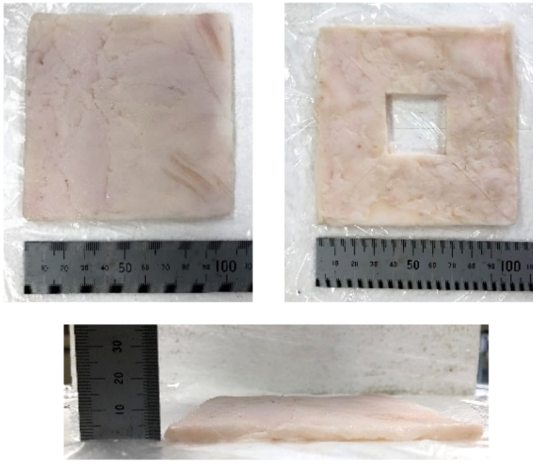

Fig. 15 Processed porcine fat.

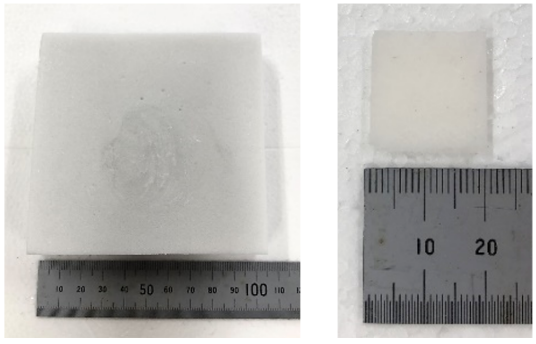

Fig. 16 Muscle phantom and blood phantom.

muscle and blood are both high water content tissues, we used the TX-151 phantom, which was relatively easy to fabricate, for both muscle and blood. The muscle phantom was fabricated based on the composition of the 2/3 muscle phantom for the UWB band [17]. The blood phantom was also prepared by adjusting the amount of the same material.

Finally, the hybrid phantom combining the above is

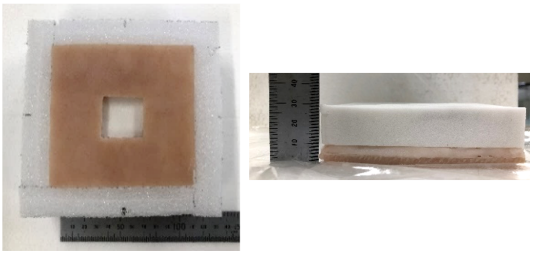

Fig. 17 Hybrid phantom.

Table 3 Target electrical constants.

Tissues and phantoms	Relative permittivity ε_r		Conductivity σ [S/m]	
	Target	Meas.	Target	Meas.
Skin	32.9	23.5	9.52	8.11
Fat	4.56	3.46	0.62	0.73
Muscle	42.1	39.0	11.4	13.3
Blood	44.3	42.8	7.56	15.0

shown in Fig. 17. The skin, fat, and muscle phantoms were layered in this order and gently pressed against each other. The blood phantom was attached to the bottom of the defect. To prevent the phantom from losing its shape, a mold frame was made of Styrofoam. We made the following models by changing the combination of layer of loss (skin or fat) and the length of defect (L): Healthy skin, Skin layer loss + L = 20, Skin layer loss + L = 30, Fat layer loss + L = 20, and Fat layer loss + L = 30.

Table 3 shows the target electrical constants and measured values of each phantom/tissue. Although the error between the target value and the measured value for both the relative permittivity and the conductivity was relatively large, the experiment was conducted without changes since there was no way to make adjustments.

3.3 Experimental Environment

An overview of the experimental environment is shown in Fig. 18. A microwave network analyzer N5230C (Agilent Technologies) was used for the measurements. We set up a Styrofoam framework so that the distance from the upward-facing antenna surface to the phantom surface was 100 mm. We also adjusted the position of the phantom so that the center of the antenna was aligned with the center of the phantom. The obtained waveform was S_{11}Real, the real part of S_{11}, converted to the time domain. This can be treated equivalently to the voltage waveform in the analysis.

3.4 Experimental Results

The graphs of the time response show the results of experiments and analysis (Fig. 20). The experimental results showed a similar pattern to the analytical results, but there were slight differences. This value discrepancy may be due

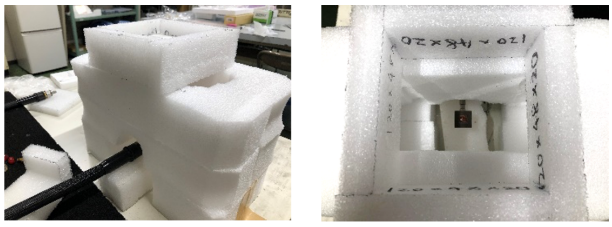

Fig. 18 Overview of experimental environment.

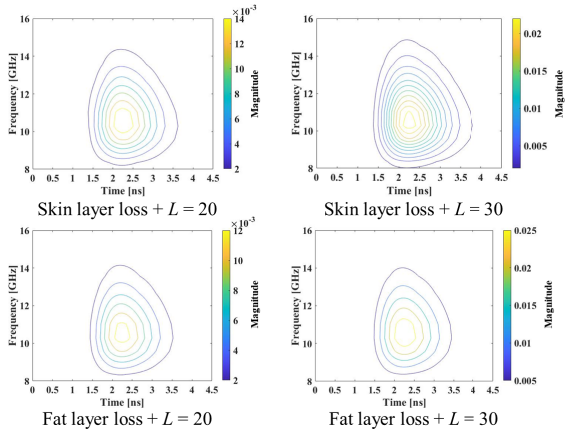

Fig. 19 Results of scalograms.

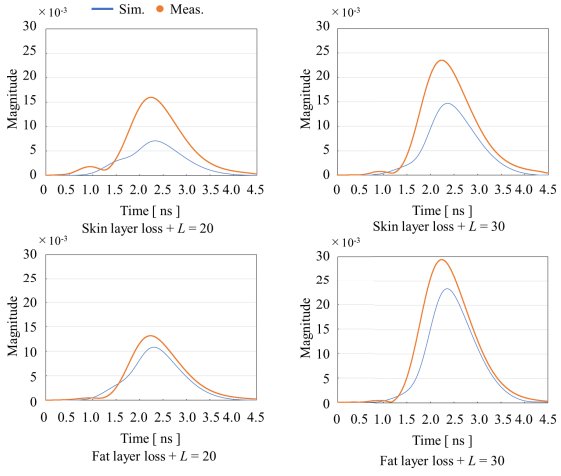

Fig. 20 Time response of the relevant frequency band extracted from the scalogram.

to the air layer between each phantom layer. The disparity in the electrical constants may be another causative factor.

However, such a difference could be sufficiently improved. Moreover, the general shapes of the graphs, including time and frequency bands, were very similar to that of the analysis, and it was possible to obtain the peak values and the reaching times necessary for detection. Based on the above, it was confirmed that the essential operation of this method was sufficiently feasible.

4. Conclusion

In this paper, we extracted appropriate information from a scalogram that was obtained by applying wavelet transformation to the waveform affected by bedsore and utilized it to detect the sizes of bedsores. If the waveform changes from a healthy skin condition, it can be determined that a Stage I or higher-bedsore has developed. However, the changes in Stage I are small, so setting a threshold to distinguish them from changes in body surface conditions is an issue to consider in the future. Moreover, using the approximate curves and lines, it was possible to convert the reaching time to an estimated volume of the defected area and convert the peak value to the estimated combinations of the depth of the defected area and the length of the defected area. In addition, the experiments showed that it was possible to detect bedsore presence and estimate their sizes, although the detection results had slight variations. These are very important findings. In the future, we plan to develop a system that enables early detection of bedsores by using models that more likely resemble the human body and also examine bedsore waveforms in more detail.

References

[1] Cabinet Office, "Annual Report on the aging Society FY2022," Japan [Online]. Available: https://www8.cao.go.jp/kourei/whitepaper/w-2022/zenbun/pdf/1s1s_01.pdf
[2] United Nations, Department of Economic and Social Affairs, Population Division (2022), "World population prospects 2022: Summary of results," pp.7–8, 2022.
[3] Japanese Nursing Association, "Nursing Challenges for 2025, Vision for the Future of Nursing~Nursing care that protects and supports Life, Livelihood and Dignity~," Japan, [Online]. Available: https://www.nurse.or.jp/home/about/vision/index.html
[4] National Pressure Ulcer Advisory Panel, European Pressure Ulcer Advisory Panel and Pan Pacific Pressure Injury Alliance, "Prevention and treatment of pressure ulcers: Quick reference guide," E. Haesler, ed., Cambridge Media: Perth, Western Australia, pp.12–13, 2014.
[5] S.L. Swisher, M.C. Lin, A. Liao, E.J. Leeflang, Y. Khan, F.J. Pavinatto, K. Mann, A. Naujokas, D. Young, S. Roy, M.R. Harrison, A.C. Arias, V. Subramanian, and M.M. Maharbiz, "Impedance sensing device enables early detection of pressure ulcers in vivo," Nat. Commun., vol.6, 6575, March 2015.
[6] H. Moghadas and V.K. Mushahwar, "Passive microwave resonant sensor for detection of deep tissue injuries," Sensors & Actuators: B. Chemical, vol.277, pp.69–77, 2018.
[7] T. Hirano, T. Kikkawa, J. Hirokawa, and M. Ando, "Wideband pentagonal patch antenna for body diagnostic," IEICE Trans. Electron. (Japanese Edition), vol.J99-C, no.8, pp.365–372, Aug. 2016.
[8] S. Shrestha, M. Agarwal, P. Ghane, and K. Varahramyan, "Flexible microstrip antenna for skin contact application," International Journal of Antennas and Propagation, vol.2012, Article ID 745426, 5 pages, 2012.
[9] O. Malyuskin and V. Fusco, "Resonance microwave reflectometry for early stage skin cancer identification," 2015 9th European Conference on Antennas and Propagation (EuCAP), Lisbon, Portugal, 2015.
[10] R. Onose, Y. Enokibori, and K. Mase, "Comparison of E-textile-based pressure sensor cloth and sheets," IPSJ Interaction 2017, pp.480–485, 2017.
[11] M. Kosaka and M. Takahashi, "Stage identification using electromagnetic waves for a noncontact bedsores detection system," 2019 In-

ternational Symposium on Antennas and Propagation (ISAP), Xi'an, China, 2019.
[12] H. Kobayashi and M. Takahashi, "Identification of bedsore using electromagnetic waves for a noncontact detection system," 2021 International Symposium on Antennas and Propagation (ISAP), Taipei, Taiwan, 2021.
[13] Y. Asano and M. Takahashi, "Development of a microwave bedsore detection method using wavelet transforms," 2022 IEEE International Workshop on Electromagnetics (iWEM), Narashino, Chiba, Japan, 2022.
[14] Ministry of Internal Affairs and Communications, "Frequency Assignment Plan (as of September 2022)," 2022, Japan, [Online]. Available: https://www.tele.soumu.go.jp/e/adm/freq/search/share/plan.htm
[15] H. Sanada, K. Yabunaka, G. Nakagami, and T. Sakamoto, "Biological tissue models and human body models for bedsore diagnosis and training," JP Patent P2016-224396A, Dec. 28, 2016.
[16] Japanese Society of Pressure Ulcers, "Revised DESIGN-R®2020 Consensus Document," Shorinsha, Japan, 2020.
[17] J. Zhou, D. Hara, and T. Kobayashi, "Development of ultra wideband electromagnetic phantoms for antennas and propagation studies," European Conference on Antennas and Propagation, Nice, France, 2006.

Tomoki Chiba was born in Mie, Japan, in 1999. He received the B.Eng. degree from Chiba University, Chiba, Japan in 2022. He is currently pursuing the M.Eng. degree at Chiba University, engaging in research on a non-contact bedsore detection system.

Yusuke Asano was born in Akita, Japan, in 1998. He received the B.Eng. and M.Eng. degree from Chiba University, Chiba, Japan in 2021 and in 2023.

Masaharu Takahashi was born in Chiba, Japan, in December 1965. He received the B.Eng. degree in electrical engineering from Tohoku University, Miyagi, Japan, in 1989, and the M.Eng. and D.Eng. degrees in electrical engineering from Tokyo Institute of Technology, Tokyo, Japan, in 1991 and 1994, respectively. From 1994 to 1996, he was a Research Associate, and from 1996 to 2000, an Assistant Professor with Musashi Institute of Technology, Tokyo, Japan. From 2000 to 2004, he was an Associate Professor with Tokyo University of Agriculture and Technology, Tokyo, Japan. He is currently an Associate Professor with the Research Center for Frontier Medical Engineering, Chiba University, Chiba, Japan. He served as Editor-in-Chief of IEICE Transactions on Communication from 2011 to 2013, Vice Chair of Editorial Board, IEICE Communication Society from 2013 to 2014, Editor in chief of Editorial committee of IEICE Communications Society Magazine (Japanese Edition) from 2014 to 2016, Chair of Technical Committee on Wireless Power Transfer, IEICE from 2018 to 2020, Vice President of IEICE-CS Board from 2019 to 2021, Chair of IEEE Antennas & Propagation Society Tokyo Chapter from 2019 to 2020, and General Co-Chair of iWEM2022. His main interests are electrically small antennas, planar array antennas, and EM compatibility. He was the recipient of the 1994 IEEE Antennas and Propagation Society (IEEE AP-S) Tokyo Chapter Young Engineer Award.